Nonlinear Analysis of Charge-Pump Phase-Locked Loop: The Hold-In and Pull-In Ranges

Nikolay Kuznetsov, Alexey Matveev, Marat Yuldashev, and Renat Yuldashev

Dedicated to the memory of IEEE fellow Floyd M. Gardner (1929 – 2021).

***Abstract*— In this paper a fairly complete mathematical model of CP-PLL, which reliable enough to serve as a tool for credible analysis of dynamical properties of these circuits, is studied. We refine relevant mathematical definitions of the hold-in and pull-in ranges related to the local and global stability. Stability analysis of the steady state for the charge-pump phase locked loop is non-trivial: straight-forward linearization of available CP-PLL models may lead to incorrect conclusions, because the system is not smooth near the steady state and may experience overload. In this work necessary details for local stability analysis are presented and the hold-in range is computed. An upper estimate of the pull-in range is obtained via the analysis of limit cycles. The study provided an answer to Gardner's conjecture on the similarity of transient responses of CP-PLL and equivalent classical PLL and to conjectures on the infinite pull-in range of CP-PLL with proportionally-integrating filter.**

***Index Terms*— Charge-pump PLL, CP-PLL, phase-locked loops, VCO overload, Gardner conjecture, hidden oscillations.**

I. Introduction

DESIGN and analysis of frequency control circuits is a challenging task relevant to many applications: satellite navigation [1], digital communication [2], wireless networks [3], to mention just a few. Effective locking onto the phase of the input signal is among the principal problems solved by means of such circuits. From a broad perspective, their synthesis and analysis fall under the framework of standard topics in control engineering like signal tracking, linear and global stability. Meanwhile, some of ubiquitous and actively used circuits are largely inspired by implementability issues and approaches of practical control engineering so that their true capacities and limitations still await fully disclosing via a rigorous analysis.

This paper aims at filling this gap with respect to the Charge-Pump Phase-Locked Loop (CP-PLL), which is used for frequency synthesis and clock generation in computer architectures [4]. The CP-PLL is able to quickly lock onto the phase of the incoming signal, achieving low steady-state phase error. Stability of the CP-PLL steady state (the locked state) was originally studied by F. Gardner in [5] using approximate linear models. In this pioneering work he conjectured that *transient response of practical charge-pump PLL's can be expected to be nearly the same as the response of the equivalent classical PLL*. Later on, approximate discrete-time linear models of the CP-PLL were suggested in [6], [7]. The closed loop nonlinear discrete time model of CP-PLL was suggested in [8]. In this paper we develop, augment, and supplement the approach used in the reported literature in order to extend it to the practically important case of Voltage Controlled Oscillator (VCO) overload (see, e.g. [9], [10]).

The range of input frequencies associated with stable steady state corresponds to the hold-in range. For the classical analog PLL, stability of the locked state depends on the gap between the VCO free-running frequency and the frequency of the reference signal. For first-order active proportionally-integrating (PI) filter, analog PLL is theoretically stable for any gap [11]. Conversely, stability of the locked state of CP-PLL depends on the reference frequency even if PI loop filter is employed. Moreover, the CP-PLL is stable only for relatively high input frequencies, which is far different from that with stability of analog PLLs. It follows that even the definitions of the hold-in, the pull-in and the lock-in ranges (see, e.g. [12]–[15]) should be refined for the CP-PLL, to say nothing about the need to update and extend the base of relevant knowledge about the properties of the circuit. Note, that it is important to know how VCO overload limits stability, because CP-PLL may not operate correctly near the overload due to non-linearities of voltage-frequency characteristics. From practical point of view overload should be avoided, since it may break circuits or lead to unpredicted behaviour [16]. Therefore it is important to find parameters which may lead to overload and understand how to identify oscillations tied to it.

Extra troubles stem from the fact that straight-forward linearization of available CP-PLL models may lead to incorrect conclusions, because the system is not smooth near the steady state (in fact, it is only piecewise smooth). In [17], stability analysis follows the lines of a Lyapunov approach, however,

Manuscript received February 27, 2021; revised June 12, 2021; accepted July 14, 2021. This work was supported in part by the Russian Science Foundation under Project 19-41-02002 and in part by the Leading Scientific Schools of Russia Project under Grant NSh-2624.2020.1 (publication fee). This article was recommended by Associate Editor J. Juillard. *(Corresponding author: Nikolay Kuznetsov.)*

Nikolay Kuznetsov is with the Faculty of Mathematics and Mechanics, Saint-Petersburg State University, 199034 Saint Petersburg, Russia, also with the Faculty of Information Technology, University of Jyväskylä, 40014 Jyväskylä, Finland, and also with the Institute for Problems in Mechanical Engineering, Russian Academy of Science, 199178 Saint Petersburg, Russia (e-mail: nkuznetsov239@gmail.com).

Alexey Matveev, Marat Yuldashev, and Renat Yuldashev are with the Faculty of Mathematics and Mechanics, Saint-Petersburg State University, 199034 Saint Petersburg, Russia.

Color versions of one or more figures in this article are available at https://doi.org/10.1109/TCSI.2021.3101529.

Digital Object Identifier 10.1109/TCSI.2021.3101529

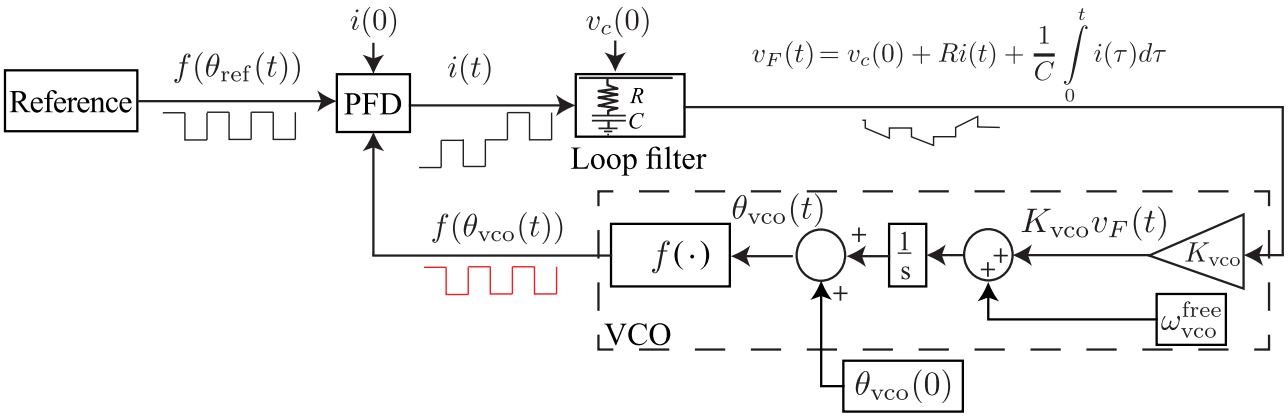

Fig. 1. Charge-pump PLL.

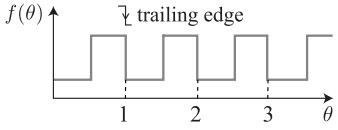

Fig. 2. Waveform of the reference and VCO signals.

details of the proof are not presented. Note that nonlinear high-order mathematical models of CP-PLL can also be built by using approximations of exponentials (see, e.g. [18]–[25]), but the resulting transcendental equations cannot be solved analytically without using approximations.

In this paper, we use the findings of [26] as a keystone, and develop, augment, and supplement them in order to acquire a fairly complete mathematical model of CP-PLL reliable enough to serve as a tool for credible analysis of dynamical properties of these circuits. To this end, we also refine some relevant mathematical definitions of main characteristics, and demonstrate the potentiality of the proposed model.

II. Mathematical Model of the Charge-Pump Phase-Locked Loop With Phase-Frequency Detector

Consider the charge-pump phase-locked loop with phase-frequency detector [5], [27] in Fig. 1. Both the reference (Ref) and output of the VCO are square waveform signals (Fig. 2) with phases $\theta_{\rm ref}(t)$ and $\theta_{\rm vco}(t)$, respectively. Without loss of generality we suppose that trailing edges of the VCO and reference signals occur when the corresponding phase reaches an integer number. The frequency $\omega_{\rm ref} > 0$ of reference signal (reference frequency) is usually assumed to be constant:

$$\theta_{\rm ref}(t) = \omega_{\rm ref} t = \frac{t}{T_{\rm ref}}, \tag{1}$$

where $T_{\rm ref} > 0$ is a period of the reference signal.

The Phase-Frequency Detector (PFD) is a digital circuit, triggered by the trailing (falling) edges of the Ref and VCO signals. The output signal of PFD $i(t)$ can have only three states (Fig. 3): 0, $+I_p$, and $-I_p$. A trailing edge of the reference signal forces the PFD to switch to a higher state, unless it is already in the state $+I_p$.

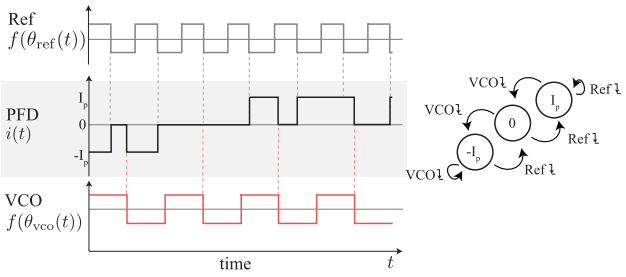

Fig. 3. Phase-frequency detector operation.

A trailing edge of the VCO signal forces the PFD to switch to a lower state, unless it is already in the state $-I_p$. If both trailing edges happen at the same time, then the PFD switches to zero. Therefore, for positive frequencies the PFD output $i(t)$ always returns to zero from non-zero state at certain time. Thus, without loss of generality, assume that $i(t) = 0$ till the time $t = 0$ (i.e. $i(0-) = i(0) = 0$) when for the first time one of trailing edge appears at the input of the PFD. For $t > 0$ the function $i(t)$ is determined by $i(t-)$, $\theta_{\rm vco}(t)$, and $\theta_{\rm ref}(t)$.

The relationship between the input current $i(t)$ and the output voltage $v_F(t)$ for a proportionally integrating (perfect PI) filter based on resistor and capacitor is as follows

$$v_F(t) = v_c(0) + Ri(t) + \frac{1}{C}\int_0^t i(\tau)d\tau, \tag{2}$$

where $R > 0$ is a resistance, $C > 0$ is a capacitance, and $v_c(t) = v_c(0) + \frac{1}{C}\int_0^t i(\tau)d\tau$ is a capacitor charge; the transfer function is $H(s) = R + \frac{1}{Cs}$.

The control signal $v_F(t)$ adjusts the VCO frequency:

$$\dot\theta_{\rm vco}(t) = \omega_{\rm vco}(t) = \omega_{\rm vco}^{\rm free} + K_{\rm vco}v_F(t), \tag{3}$$

where $\omega_{\rm vco}^{\rm free}$ is the VCO free-running (quiescent) frequency (i.e. for $v_F(t) \equiv 0$), $K_{\rm vco}$ is the VCO gain (sensitivity).

Consider one important thing regarding the charge-pump (CP) using in the PFD: transistors inside CP reasonably approximates the current generators until the drain-source voltage magnitude is higher than a given minimum value.

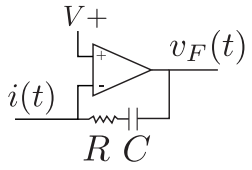

Fig. 4. Loop filter with operational amplifier: the transfer function $H(s) = I_p(R + (Cs)^{-1})$.

Note that both transistors' output characteristics approximate the current generators only if the output voltage is within the current saturation region. The CP-PLL will work as expected only if the CP output voltage is within its valid range. In order to keep both transistors within their current saturation region, a "zero impedance" (or very low) to ground (or to any DC voltage) is needed. This means that the loop filter has to have a capacitor to GND if it is purely passive. One of the simplest solutions is to use a second-order filter. Here we consider another solution: to add operational amplifier to the filter [16] (see Fig. 4). In this case the transfer function of the loop filter remains the same as in (2).

From (1), (2), and (3), for the given ω_{ref} we obtain a *continuous time nonlinear mathematical model of CP-PLL* described by the following differential equations

$$\dot{v}_c(t) = \tfrac{1}{C} i(t), \quad \dot{\theta}_{\text{vco}}(t) = \omega_{\text{vco}}^{\text{free}} + K_{\text{vco}}\,(Ri(t) + v_c(t)) \quad (4)$$

with the discontinuous, piecewise constant nonlinearity $i(t) = i\big(i(t-), \omega_{\text{ref}}, \theta_{\text{vco}}(t)\big)$ and initial conditions $\big(v_c(0), \theta_{\text{vco}}(0)\big)$. This model is nonlinear, non-autonomous, discontinuous, and switching system which is hard to analyze.

A. Overload

Depending on the design, the VCO input in CP-PLL may experience overload (see, e.g. [8], [10], [16]). From the mathematical point of view the VCO overload means that frequency is driven to a non-positive value, i.e at some point t'

$$\dot{\theta}_{\text{vco}}(t') = \omega_{\text{vco}}^{\text{free}} + K_{\text{vco}}\left(Ri(t') + v_c(t')\right) \le 0. \quad (5)$$

B. Locked States

If the synchronization is achieved, i.e. a transient process is over, then the loop is said to be in a *locked state*. When CP-PLL is in a locked state, the trailing edges of the VCO signal happen almost at the same time as the trailing edges of the reference signal. In a locked state the output of PFD $i(t)$ can be non-zero only on short time intervals (shorter than τ_{lock}). The allowed residual phase difference τ_{lock} should be in agreement with engineering requirements for a particular application. We consider the ideal case $\tau_{\text{lock}} = 0$.

III. Nonlinear Discrete Time CP-PLL Model

For nonlinear analysis, we pass from model (4) to a discrete-time model. Following [26], we derive a discrete time model of the CP-PLL. Without loss of generality, assume that $i(t) = 0$ till the time t_0 (i.e. $i(t_0) = 0$) when for the first time one of trailing edge appears at the input of the PFD. If only one

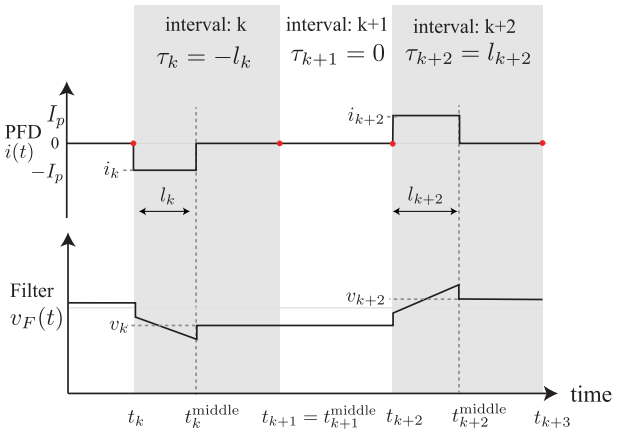

Fig. 5. Discrete states τ_k and v_k; l_k is the PFD pulse width.

of the trailing edges appear, the PFD output becomes non-zero (i.e. $i(t_0+) \neq 0$), and then we denote by $t_0^{\text{middle}} > t_0$ the first instant of time such that the PFD output becomes zero (i.e. $i(t_0^{\text{middle}}) = 0$). If both VCO and Ref trailing edges appear at the same time, we denote $t_0^{\text{middle}} = t_0$. Then, we wait until the first trailing edge of the VCO or Ref, and denote the corresponding moment of time by t_1 (i.e. $i(t_1) = 0$). Continuing in a similar way, one obtains the increasing sequences $\{t_k\}$ and $\{t_k^{\text{middle}}\}$ for $k = 0, 1, 2\ldots$ Thus, $i(t) = 0$ for $t_k^{\text{middle}} \le t \le t_{k+1}$ and $i(t) = \pm I_p$ for $t_k < t < t_k^{\text{middle}}$. Denote by τ_k the PFD pulse width (length of the time interval, where the PFD output is a non-zero constant) multiplied by the sign of the PFD output (see Fig. 5):

$$\tau_k = \left(t_k^{\text{middle}} - t_k\right) \text{sign}\left(i\left(\frac{t_k + t_k^{\text{middle}}}{2}\right)\right). \quad (6)$$

If the VCO trailing edge hits before the Ref trailing edge then $\tau_k < 0$, in the opposite case we have $\tau_k > 0$. Thus, τ_k shows how one signal lags behind another.

From (2) it follows that the zero output of PFD $i(t) \equiv 0$ on the interval $[t_k^{\text{middle}}, t_{k+1}]$ implies a constant filter output. Denote this constant by v_k. We have

$$v_F(t) \equiv v_k, \quad t \in [t_k^{\text{middle}}, t_{k+1}]. \quad (7)$$

Following the ideas from [17], [28], denote

$$p_k = \frac{\tau_k}{T_{\text{ref}}}, \quad u_k = T_{\text{ref}}\left(\omega_{\text{vco}}^{\text{free}} + K_{\text{vco}} v_k\right) - 1,$$

$$\alpha = K_{\text{vco}} I_p T_{\text{ref}} R > 0, \quad \beta = \frac{K_{\text{vco}} I_p T_{\text{ref}}^2}{2C} > 0. \quad (8)$$

Here p_k is a normalized phase shift and $u_k + 1$ is a ratio of the VCO frequency $\omega_{\text{vco}}^{\text{free}} + K_{\text{vco}} v_k$ to the Ref frequency $\frac{1}{T_{\text{ref}}}$.

A. Overload

Condition (5) of the VCO overload on $[t_k, t_{k+1})$ corresponds to the following cases:

- for $\tau_k < 0$ one can see from Fig. 6 that the VCO is overloaded for

$$\inf_{t \in [t_k, t_{k+1})} \dot{\theta}_{\text{vco}}(t) = \omega_{\text{vco}}^{\text{free}} + K_{\text{vco}}(v_c(t_k) + \tau_k \tfrac{I_p}{C} - I_p R) \le 0; \quad (9)$$

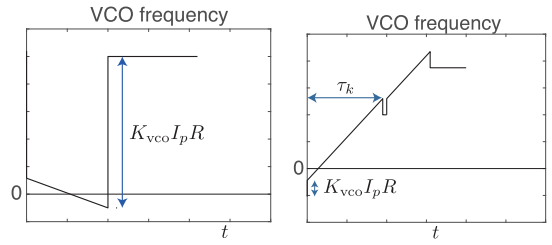

Fig. 6. VCO overload near the locked state: a) for $\tau_k < 0$ b) for $0 < \tau_k < 1$.

- for $\tau_k \geq 0$, the VCO may be also overloaded initially, see Fig. 6:

$$\inf_{t\in[t_k,t_{k+1})} \dot{\theta}_{\rm vco}(t) = \omega_{\rm vco}^{\rm free} + K_{\rm vco}\upsilon_c(t_k) \leq 0. \qquad (10)$$

In practice the VCO overload should be avoided (see, e.g. [8], [16]). From the mathematical point of view a task may be posed to find the biggest positively invariable region of phase space in which there is no overload. However, for any parameters R, C, $K_{\rm vco}$, and I_p the VCO overload may occur for sufficiently large frequency difference between the VCO and reference signals. Therefore, it is reasonable to demand that at least for the same frequencies of the Ref and VCO signals and small time delay between signals there is no overload. For locked state, i.e. for $\tau_k = 0$ and the same frequencies, inequality (10) cannot be valid for $T_{\rm ref} > 0$. Thus, theoretically, in a locked state the VCO is not overloaded. However the VCO can be overloaded near the locked state (*local overload*) for any small width pulses on the output of the PFD. Therefore, both equations (9) and (10) should be checked. Substituting $\frac{1}{T_{\rm ref}} = \omega_{\rm vco}^{\rm free} + K_{\rm vco}\upsilon_c(t_k)$ into (9) and (10) for $\tau_k \to 0$ we get

$$\frac{1}{T_{\rm ref}} - K_{\rm vco}I_pR \leq 0, \quad \text{i.e. } \alpha \geq 1. \qquad (11)$$

Therefore, under following condition on the period of the input signal: $0 < T_{\rm ref} < T_{\rm overload}^{\rm local} = \frac{1}{K_{\rm vco}I_pR}$, there is no local overload. It may also be necessary to avoid the VCO overload even if the initial frequencies are equal but there is large time delay between signals, e.g. at startup or if the time delay between signals is changed due to a noise or period jump of the reference signal (*startup overload*). Using equal initial VCO and reference frequencies $\omega_{\rm vco}^{\rm free} + K_{\rm vco}\upsilon_c(0) = \frac{1}{T_{\rm ref}}$ in combination with (9) and (10) and assuming the worst case $\tau_1 = -T_{\rm ref}$ we get startup overload condition

$$1 - \frac{K_{\rm vco}I_pT_{\rm ref}^2}{C} - K_{\rm vco}I_pT_{\rm ref}R \leq 0, \quad \text{i.e. } 1-2\beta-\alpha \leq 0. \quad (12)$$

Thus, to avoid startup overload one should choose

$$0 < T_{\rm ref} < T_{\rm overload}^{\rm startup} = \frac{-RC + \sqrt{(RC)^2 + 4\frac{C}{K_{\rm vco}I_p}}}{2}, \quad \text{i.e. } \alpha < 1 - 2\beta. \qquad (13)$$

B. CP-PLL Discrete Time Equations

Final system of equations: $x_{k+1} = f(x_k), x_k = (u_k; p_k)$, describing CP-PLL outside of the VCO overload is obtained

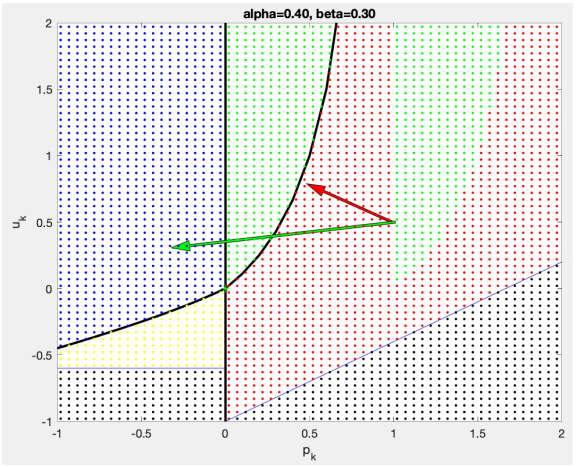

Fig. 7. Red dots: $p_k > 0$, $c_k = c(p_k, u_k) < 0$, $p_{k+1} > 0$. Green dots: $p_k > 0$, $c_k = c(p_k, u_k) > 0$, $p_{k+1} < 0$. Blue dots: $p_k < 0$, $l_k = l(p_k, u_k) < 1$, $p_{k+1} < 0$. Yellow dots: $p_k < 0$, $l_k = l(p_k, u_k) < 1$, $p_{k+1} > 0$. Black dots: VCO input overload. Red arrow: $p_k = 0.99$, $u_k = 0.5 \to p_{k+1} = 0.48$, $u_{k+1} = 0.79$. Green arrow: $p_k = 1.01$, $u_k = 0.5 \to p_{k+1} = -0.32$, $u_{k+1} = 0.31$.

from (4), (6)—(8) as follows (see [10] for details)[1]

$$u_{k+1} = u_k + 2\beta p_{k+1},$$
$$p_{k+1} = \begin{cases} \frac{-(u_k+\alpha+1)+\sqrt{(u_k+\alpha+1)^2-4\beta c_k}}{2\beta}, \\ \qquad \text{for } p_k \geq 0, \quad c_k \leq 0, \\ \frac{1}{u_k+1} - 1 + (p_k \bmod 1), \\ \qquad \text{for } p_k \geq 0, \quad c_k > 0, \\ l_k - 1, \\ \qquad \text{for } p_k < 0, \quad l_k \leq 1, \\ \frac{-(u_k+\alpha+1)+\sqrt{(u_k+\alpha+1)^2-4\beta d_k}}{2\beta}, \\ \qquad \text{for } p_k < 0, \quad l_k > 1, \end{cases} \qquad (14)$$

where

$$c_k = (1 - (p_k \bmod 1))(u_k + 1) - 1,$$
$$S_{l_k} = -(u_k - \alpha + 1)\, p_k + \beta p_k^2,$$
$$l_k = \frac{1 - (S_{l_k} \bmod 1)}{u_k + 1}, \quad d_k = (S_{l_k} \bmod 1) + u_k.$$

One of the advantages of (14) is that it has the only one steady state at $(u_k = 0, p_k = 0)$. For practical purposes, only *locally (asymptotically) stable steady state*, in which the loop returns after small perturbations of its state, is of interest.

Note that the right-hand side of (14) is continuous and piecewise smooth in neighborhood of the origin and discon-

[1]The differences between model (14) and the models from [17] and [8] can be demonstrated, for example, as follows. The values $\alpha = 0.2$, $\beta = 1.7$, $p_0 = -0.18$ and $u_0 = -0.43$ are not taken into account in [17] where the corresponding values $a = \alpha$, $b = \beta$, $\hat{\tau}_k = p_k$, and $\upsilon_k = u_k$ are outside of the allowed area in Fig. 2.a [17, page 1114]. The values $R = 0.2$, $C = 0.01$, $K_{\rm vco} = 20$, $I_p = 0.1$, $T_{\rm ref} = 0.125$, $\tau_0 = 0.0125$, and $\upsilon_0 = 1$ correspond to the VCO overload, while in [8] the consideration of the corresponding values $R_2 = 0.2$, $C = 0.01$, $K_v = 20$, $I_p = 0.1$, $T = 0.125$, $\tau(0) = 0.0125$, $\upsilon(0) = 1$ leads to extracting of the square root from -1, i.e. $\sqrt{-1}$ (the editors of IEEE TCOM journal, where two pioneering works [5] and [8] on the CP-PLL had been published, were notified about the above problem and discussed results but did not provide a way to inform journal's readers). See details in [26].

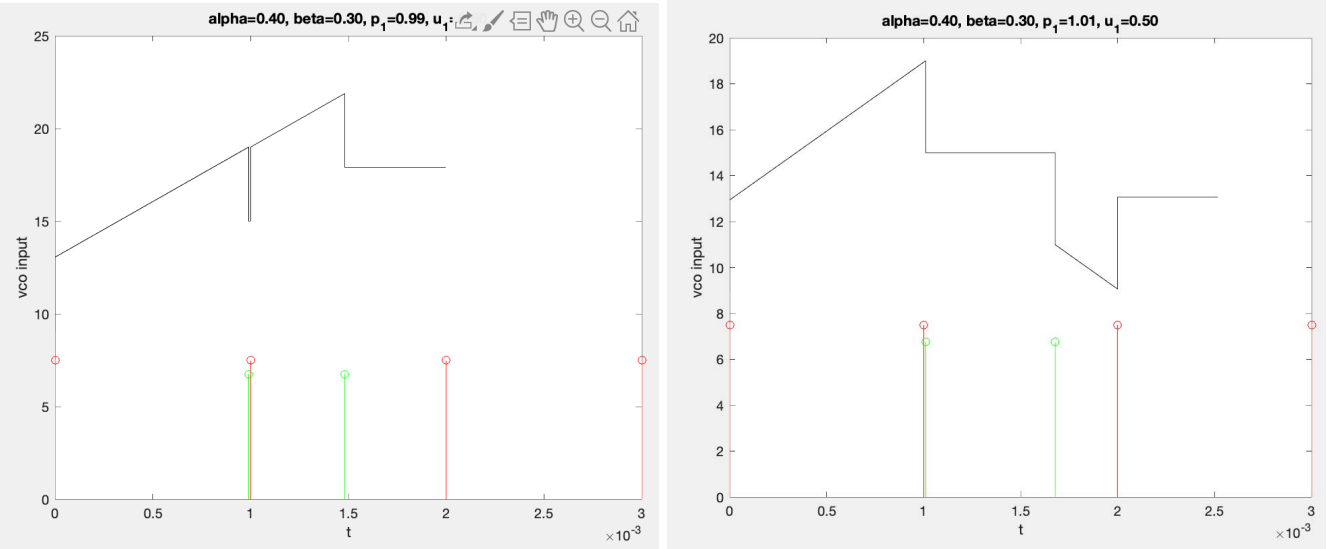

Fig. 8. Quantitative difference in PFD behaviour for small difference of phases. Red — reference trailing edges; green — VCO trailing edges. Black — VCO input. Left: $p_k = 0.99,\ u_k = 0.5 \ \rightarrow \ p_{k+1} = 0.48,\ u_{k+1} = 0.79$. Right: $p_k = 1.01,\ u_k = 0.5 \ \rightarrow \ p_{k+1} = -0.32,\ u_{k+1} = 0.31$.

tinuous far from the origin (see Fig. 7 and the corresponding VCO input signals in Fig. 8).

IV. Small-Signal Analysis: The Locked State

The local stability analysis of the CP-PLL model via straight-forward linearization may lead to incorrect conclusions because the system is not smooth near the steady state (in fact, it is only piecewise smooth). In [17], [29] the stability analysis follows the lines of the Lyapunov approach, however, the details of the proof are not presented[2] and the analysis is done without taking into account the VCO overload.

Model (14) has only one steady state

$$u_k = u_{k+1} \equiv 0, \quad p_k = p_{k+1} \equiv 0, \tag{15}$$

which is a locked state if the state is locally asymptotically stable. In [10], [26] it is shown that a small vicinity of the zero steady state lies outside the VCO overload if condition $0 < \alpha < 1$ holds (thus we can use model (14) for the local analysis of the loop).

V. The Hold-In Range of CP-PLL

The hold-in range corresponds to the input frequency range, which allows PLL to keep acquired locked state despite small and slow deviations of the input frequency or phase. This notion is similar to the definition of the hold-in range for classic analog PLLs [12]–[14]. However, as shown below, for the considered CP-PLL model there is always a reference signal period T_{ref} such that the steady state $u_k = p_k = 0$ is stable (assuming that there is no overload). Moreover, for any smaller values of T_{ref} the equilibrium $u_k = p_k = 0$ remains locally stable. Therefore, it is reasonable to give the following definition of the hold-in range for the CP-PLLs.

Definition 1: The hold-in range of the CP-PLL is a maximum range of the input signal periods $T_{\text{ref}} = \frac{1}{\omega_{\text{ref}}}$*:*

$$0 < T_{\text{ref}} < T_{\text{hold-in}}, \tag{16}$$

such that there exists a locked state (i.e., an asymptotically stable steady state of nonlinear discrete time CP-PLL model (14)*) near which the VCO is not overloaded.*

Here, $\omega_{\text{vco}}^{\text{free}}$ does not affect the hold-in range and can be predetermined for certainty. Since it is not possible to choose zero value $\omega_{\text{vco}}^{\text{free}} = 0$ (because in this case the transistors inside the charge-pump do not operate properly), one can choose $\omega_{\text{vco}}^{\text{free}} = \frac{1}{T_{\text{hold-in}}}$ or equal to the expected frequency of the reference signal. The stability of the steady state for $0 < \alpha < 1$ (no local overload condition) and $0 < \beta < 2$ is proved in Appendix B. Then, substituting $T_{\text{ref}} = \sqrt{\frac{2C\beta}{K_v I_p}}$ and $T_{\text{ref}} = \frac{\alpha}{K_{\text{vco}} I_p R}$ from (8) into the above inequalities we obtain estimate (17). The proof is based on sufficient conditions for stability (as in classical results on stability by the first approximation for nonlinear ODE), at the same time for $\beta > 2$ the linearized system becomes unstable and numerical simulation shows that the origin of nonlinear model (14) becomes unstable (see corresponding discussion in Appendix C and in Fig. 9), thus the equality is stated in the theorem.

Theorem 1: The hold-in range of CP-PLL is as follows

$$\frac{1}{\omega_{\text{ref}}} = T_{\text{ref}} < T_{\text{hold-in}} = \min\left\{\sqrt{\frac{4C}{K_{\text{vco}} I_p}}, \frac{1}{K_{\text{vco}} I_p R}\right\}. \tag{17}$$

Remark that (17) refines the estimate that can be obtained according to Definition 1 from the results in [17], which do not take into account the overload: $T_{\text{hold-in}} \geq \sqrt{\frac{4C}{K_{\text{vco}} I_p}}$.

VI. The Pull-In Range and Non-Local Analysis

Following the Gardner's conjecture on CP-PLL [5, p.1856] and the Egan conjecture on the pull-in range of type 2 APLL [30, p.176], [11], [31], in [32, p.6] it was noted that in order to have an infinite pull-in range in CP-PLL, an active filter must be used for the loop filter (i.e. in this case the pull-in range is only limited by the VCO tuning range [33, p.32], [34, p.29]). However, unlike classic PLLs with PI filter [15], [35], for some parameters and initial input frequencies the

[2]"The proof of this assertion is neither trivial nor brief" [17, p.9].

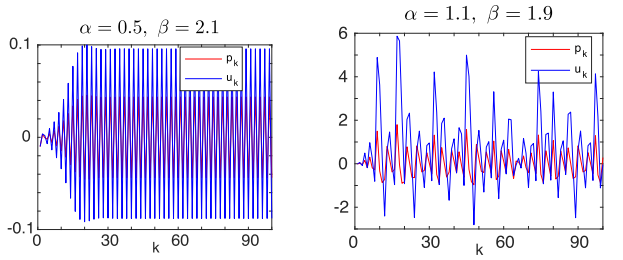

(a) origin is unstable for $\beta > 2$. Simulation of model (14), $\alpha = 0.5, \beta = 0.1$

(b) origin is unstable for $\alpha > 1$ simulation of model taking into account overload from [10], $\alpha = 1.1, \beta = 1.9$

Fig. 9. Numerical simulation of local stability, $p_0 = u_0 = -0.01$.

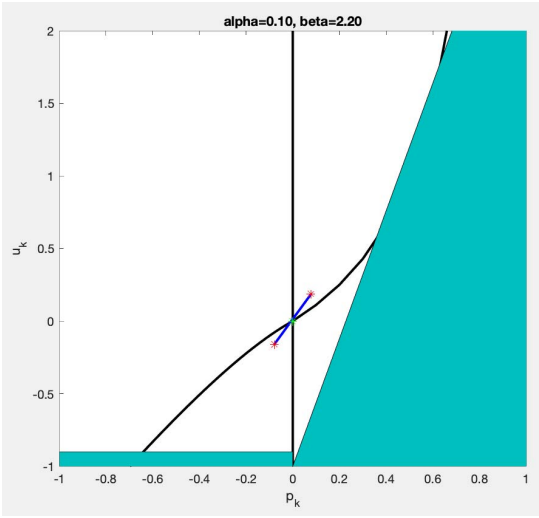

Fig. 10. Period-2 limit cycle. Red stars: limit cycle; turquoise: overload; black curves: separation of the smoothness regions.

CP-PLL cannot acquire the locked state due to the presense of nontrivial oscillations (attractors) in the phase space.

In discrete time model (14) the period-2 limit cycles have the form:

$$p_0 = \frac{-\sqrt{\beta} + \sqrt{9\beta - 16}}{4\sqrt{\beta}} > 0, \quad u_0 = \frac{2p_0}{1 - 2p_0},$$
$$p_1 = -p_0, \quad u_1 = u_0 + 2\beta p_1. \tag{18}$$

These period-2 limit cycles do not exist for $0 < \beta < 2$ (see Fig. 11, Fig. 10).

Also, there are period-3 limit cycles of the form (see Fig. 12)

$$p_0 = 0, \quad u_0 = \frac{2\beta - 3 + \sqrt{2\beta}\sqrt{2\beta - 3}}{3},$$
$$p_1 = -\frac{u_0}{u_0 + 1}, \quad u_1 = u_0 - 2\beta\frac{u_0}{1 + u_0},$$
$$p_2 = -p_1 = \frac{u_0}{1 + u_0}, \quad u_2 = u_0, \tag{19}$$

where it is assumed that $u_1 > 1 - \alpha$ and $u_2 > 2\beta p_2 - 1$ to avoid the VCO overload. Note that these cycles exist only for $\beta > \frac{3}{2}$, and for $\beta = \frac{3}{2}$ they merge with the origin. Also unstable limit cycles may exist in the model (see, e.g. Fig. 12).

While for the discrete time model (14) the limit cycles of low-periods without overload can be easily found analytically (see, e.g. [36]), the computing of limit cycles in the case

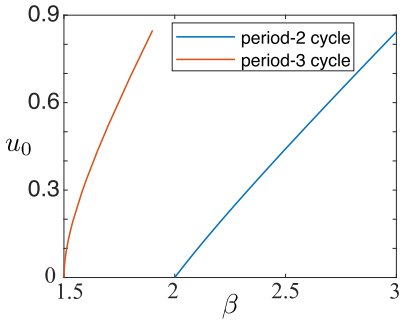

Fig. 11. Initial value u_0 corresponding to period-2 and period-3 cycles.

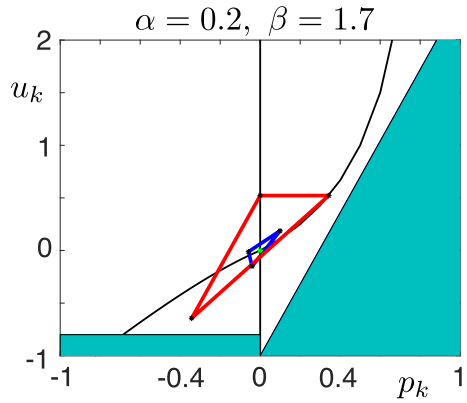

Fig. 12. Stable (red) and unstable (blue) period-3 limit cycles (hidden oscillations). Turquoise: overload; black curves: separation of the smoothness regions.

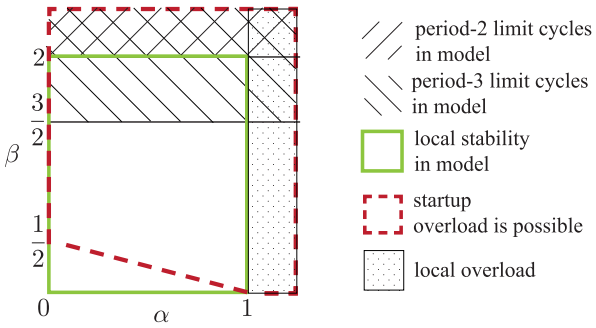

Fig. 13. Stability regions in parameter space.

of higher periods or overload leads to complicated equations which need to be solved numerically. Since the steady state is stable for $0 < \beta < 2$, $0 < \alpha < 1$, the existing limit cycles for such parameters can be classified as hidden oscillations [37], [38].

A. The Pull-In Range Estimate

For given parameters the input frequency range, for which a locked state is acquired from any possible initial state, is known as the pull-in range.

Definition 2: The pull-in range of CP-PLL is a maximum range of the input signal periods $T_{\text{ref}} = \frac{1}{\omega_{\text{ref}}}$ *within the hold-in range*:

$$0 < T_{\text{ref}} < T_{\text{pull-in}} \le T_{\text{hold-in}}, \tag{20}$$

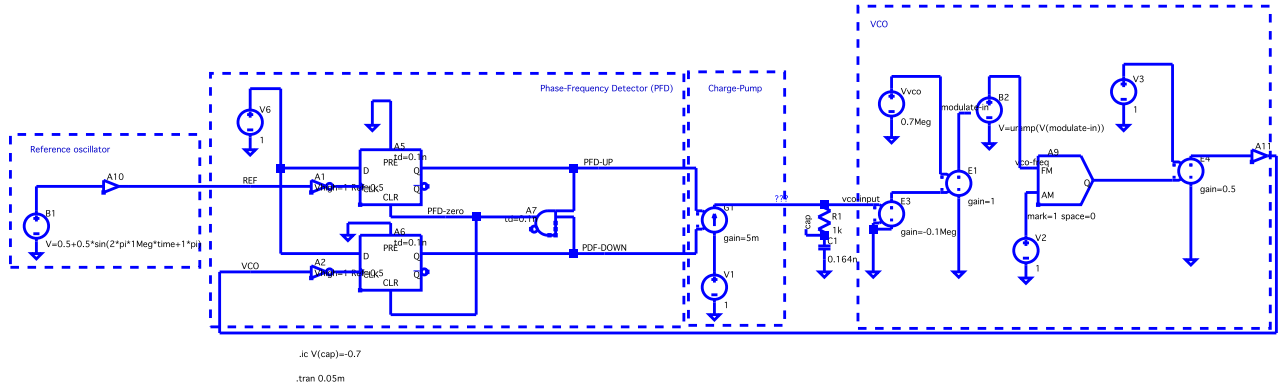

Fig. 14. LTspice schematic of CP-PLL. Circuit parameters: $R = 1\text{k}\Omega$, $C = 0.114$ nF, $\omega_{\text{ref}} = 1$ MHz, $K_{\text{vco}} = 0.1$ MHz/V, $\omega_{\text{vco}}^{\text{free}} = 0.7$ MHz, $v_c(0) = 10$ V, $\tau_0 = 0.345 \cdot 10^{-}6$ s.

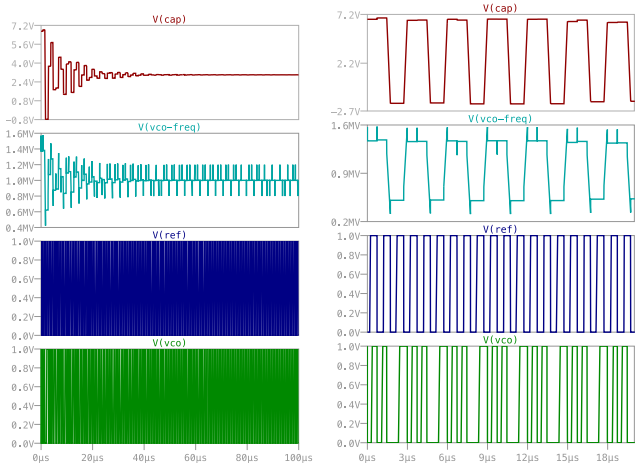

(a) $\beta = 1.4$, $C = 0.179$ nF (b) $\beta = 1.6$, $C = 0.156$ nF

Fig. 15. Birth of a stable period-3 limit cycle in LTspice for $\beta = 1.5$. Reference: "V = 0.5 + 0.5*sin(2*pi*1Meg*time − 0.45*pi)", $\omega_{\text{ref}} = 1$ MHz, $K_{\text{vco}} = 0.1$ MHz/V, $\omega_{\text{vco}}^{\text{free}} = 0.7$ MHz, $v_c(0) = 6.7$ V, $R = 0.4$ kΩ, $\alpha = 0.2$.

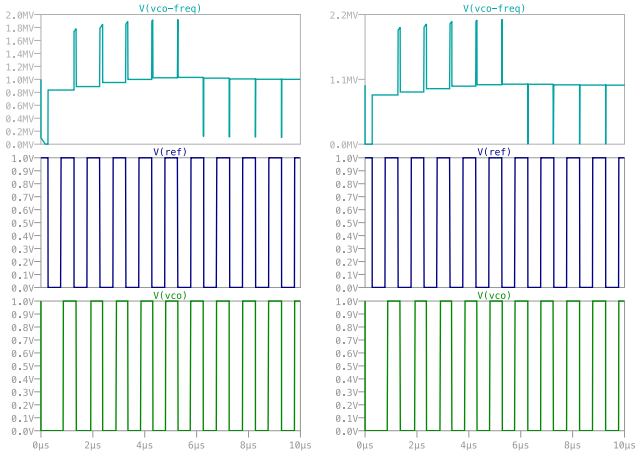

(a) $\alpha = 0.9$, $R = 1.8$ kΩ. (b) $\alpha = 1.1$, $R = 2.2$ kΩ.

Fig. 16. Local overload in LTspice for $\alpha > 1$: bursts in subfigure (b) are too large which leads to VCO overload in synchronized state. Reference: "V = 0.5 + 0.5*sin(2*pi*1Meg*time + 0.45*pi)", $\omega_{\text{ref}} = 1$ MHz, $K_{\text{vco}} = 0.1$ MHz/V, $\omega_{\text{vco}}^{\text{free}} = 1$ MHz, $v_c(0) = 6.7$ V, $C = 0.156$ nF, $\beta = 0.3$.

such that for any initial state the CP-PLL acquires a locked state.

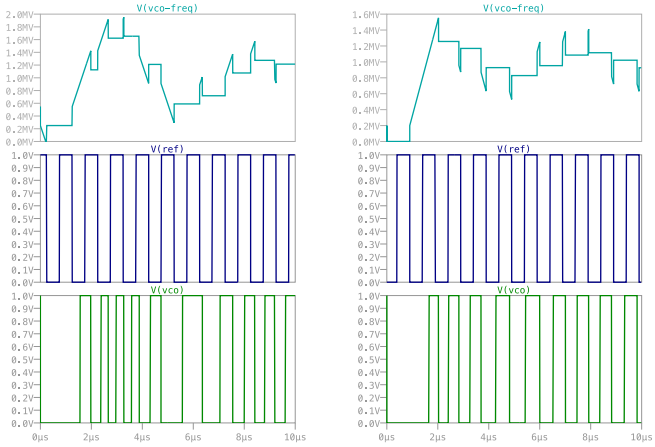

(a) $v_c(0) = -4.5$ V. (b) $v_c(0) = -11$ V.

Fig. 17. Non-local overload at startup in LTspice. $\omega_{\text{ref}} = 1$ MHz, $\omega_{\text{ref}} = 1$ MHz, $K_{\text{vco}} = 0.1$ MHz/V, $\omega_{\text{vco}}^{\text{free}} = 1$ MHz, $\alpha = 0.3$, $\beta = 0.6$, $R = 0.6$ kΩ, $C = 0.417$ nF.

Since period-2 and period-3 limit cycles exist for $\beta > \frac{3}{2}$ and $\alpha < 1$, using $T_{\text{ref}} = \sqrt{\frac{2C\beta}{K_v I_p}}$ and $T_{\text{ref}} = \frac{\alpha}{K_{\text{vco}} I_p R}$ from (8), the following upper estimate of the pull-in range can be obtained (see Fig. 13):

Theorem 2:

$$T_{\textit{pull-in}} \leq \min\left\{\sqrt{\frac{3C}{K_{\text{vco}} I_p}}, \frac{1}{K_{\text{vco}} I_p R}\right\}. \tag{21}$$

The existence of hidden periodic oscillations with higher periods or irregular oscillations may further restrict the pull-in range.[3]

Stability analysis is confirmed by the simulation in LTspice (see Fig. 14). In Fig. 15, we show that period-3 limit cycle emerges for $\beta > 1.5$. In Fig. 16, we show that VCO overload may happen in the synchronized state for $\alpha > 1$. For $\alpha < 1$ there is no overload. In Fig. 17 we show possibility of non-local overload at startup.

[3]For the classical analog PLL the birth of hidden oscillation (without loss of local stability of the locked states) may cause the loss of global stability (hidden boundary of global stability) and restrict the pull-in range [38]–[41].

VII. Conclusion

The stability of the Charge-Pump PLL has been studied for a long time. However, in these studies the VCO input overload was not fully taken into account and such important engineering parameters as the hold-in and pull-in ranges were not introduced and estimated. In this work, the definitions of the hold-in and pull-in ranges for the CP-PLL are introduced in terms of the input signal period and frequency and the corresponding estimations are discussed. We show that the VCO input overload limits the hold-in and pull-in ranges even more than the domains of parameters corresponding to linear stability and non-existence of limit cycles. The study provides an answer to Gardner's conjecture on the similarity of transient responses of CP-PLL and equivalent classical PLL [5, p.1856] and to conjectures on the pull-in range of CP-PLL with proportionally-integrating filter [32, p.6], [33, p.32], [34, p.29].

Appendix A
Local Stability for Piecewise-Smooth Systems

This section is organized in the following way. Subsection A-A considers definitions of the piecewise smooth functions. Subsection A-B states that piecewise-linear functions approximate well piecewise-smooth functions in the neighborhood of the steady state. Finally, subsection A-C proves that stability of the piecewise linearized system implies stability of the steady state for the original piecewise smooth system.

A. Piecewise-Smooth Systems

Definition 3: A hypersurface $S \subset \mathbb{R}^n$ *is a* $(n-1)$*-dimensional smooth manifold embedded in* $\mathbb{R}^n$*. Hypersurfaces* $S_1, \dots, S_k$ *are said to be* mutually non-tangential *on a subset* $O \subset \mathbb{R}^n$ *if the following claim holds*:

i) *Whenever* $x_* \in S_{i_1} \cap \dots \cap S_{i_s} \cap O$ *for some subset* $\{i_1, \dots, i_s\} \subset \{1, \dots, k\}$ *of this set* ($i_p \neq i_q \ \forall p \neq q$)*, the normals to* $S_{i_1}, \dots, S_{i_s}$ *at the point* x_* *are linearly independent.*

Definition 4: A function $f : O \subset \mathbb{R}^n \to \mathbb{R}^n$ *is said to be* piecewise smooth in a neighborhood of a point $x_* \in O$ *if there exists an open vicinity* $\mathcal{O} \subset O$ *of* x_* *and a set* $S_1, \dots, S_k$ *of hypersurfaces such that the following claims are true*:

i) *The function* $f(\cdot)$ *is continuous on* $\mathcal{O}$*;*
ii) *The function* $f(\cdot)$ *is continuously differentiable on any connected component* $\mathfrak{C}$ *of the set* $\mathcal{O} \setminus \left[S_1 \cup \dots \cup S_k\right]$ *and moreover, can be extended from* $\mathfrak{C}$ *to an open neighborhood of the closure* $\overline{\mathfrak{C}}$ *with retaining this smoothness;*
iii) *The hypersurfaces* $S_1, \dots, S_k$ *are mutually non-tangential on* $\mathcal{O}$*.*

The following is the main result of the section.

B. Linearization of the Piecewise-Smooth Function

Definition 5: A function $q : \mathbb{R}^n \to \mathbb{R}^n$ *is said to be* piecewise linear *if there exists a partition* $\mathbb{R}^n = P_1 \cup \dots \cup P_N$ *of the space* $\mathbb{R}^n$ *into finitely many polyhedral domains* P_k *such that* $q(\cdot)$ *is linear on any of them:* $q(x) = A_k x + b_k, \forall x \in P_k$.

In this section, we consider the system

$$x_{t+1} = q[x_t], \quad t = 0, 1, \dots. \tag{22}$$

under the following.

Assumption 1: The function $q(\cdot)$ *is defined on* $\mathbb{R}^n$*, continuous, piecewise linear, and positively homogeneous*

$$q(\theta x) = \theta q(x), \quad \forall x \in \mathbb{R}^n, \ \theta \in [0, \infty). \tag{23}$$

Then $q(0) = 0$, and so 0 is an equilibrium of (22). Also in Definition 5, the partition can be chosen so that any P_k is a polyhedral cone (with the vertex at the origin) and $b_k = 0$. Such a partition is said to be *conical* and q*-related*.

Definition 6: Let $f : O \to \mathbb{R}^n$ *be defined on an open subset* $O \subset \mathbb{R}^n$ *and let* $x_* \in O$ *be given. A continuous, piecewise linear, and positively homogeneous function* $q : \mathbb{R}^n \to \mathbb{R}^n$ *is called the* differential of $f(\cdot)$ *at the point* x_* *(and denoted by* $f'(x_*)$*) if*

$$\frac{f(x_* + h) - f(x_*) - q(h)}{\|h\|} \to 0 \quad \text{as} \quad h \to 0. \tag{24}$$

It is easy to check that the differential is unique (if exists) and also that the differential in the conventional sense is a particular case of the differential in the sense of Definition 6. Furthermore, (24) holds if and only if there exists a function $\alpha : \mathbb{R}^n \to \mathbb{R}^n$ such that

$$\begin{aligned} &f(x) = f(x_*) + q(x - x_*) + \|x - x_*\| \alpha(x - x_*), \\ &\alpha(h) \to 0 \quad \text{as} \quad h \to 0. \end{aligned} \tag{25}$$

Finally, the definition of the differential is invariant with respect to the choice of the norm in $\mathbb{R}^n$.

Proposition 1: Suppose that a function $f : O \subset \mathbb{R}^n \to \mathbb{R}^n$ *is piecewise smooth in a neighborhood of a point* $x_* \in O$*. Then this function has a differential* $f'(x_*)$ *in the sense of Definition* 6.

The proof of this proposition is prefaced by detailed description of this differential. To this end, we use the hypersurfaces from Definition 4. They can be given by equations of the form $S_i = \{x \in \mathcal{O} : g_i(x) = 0\}$ provided that the neighborhood $\mathcal{O}$ is properly shrunk and a smooth function $g_i : \mathcal{O} \to \mathbb{R}$ is properly chosen for any i. Moreover, this can be accomplished so that the gradient $\nabla g_i(x) \neq 0 \ \forall x \in \mathcal{O}$. Now we put

$$I := \{i = 1, \dots, k : x_* \in S_i\}$$

and define B as the set of all maps $\mathfrak{b} = \{b_i\}_{i \in I}$ that assume only two values 1 and -1. Given $\mathfrak{b} \in B$, we introduce the following sets

$$\begin{aligned} &\mathfrak{C}_\mathfrak{b} := \{x \in \mathcal{O} : b_i g_i(x) < 0 \ \forall i \in I\}, \\ &K_\mathfrak{b} := \{h \in \mathbb{R}^n : b_i h^\top \nabla g_i(x_*) \leq 0 \ \forall i \in I\}. \end{aligned} \tag{26}$$

Since $\nabla g_i(x_*)$ is the normal to S_i at point x_*, i) of Definition 3 implies that the both sets are non-empty, $x_* \in \overline{\mathfrak{C}_\mathfrak{b}}$, and $K_\mathfrak{b}$ is a polyhedral cone with the vertex at the origin. Also, $\{\mathfrak{C}_\mathfrak{b}\}_{\mathfrak{b} \in B}$ is the variety of all connected components of the set $\mathcal{O} \setminus \left[S_1 \cup \dots \cup S_k\right]$ under the condition that $\mathcal{O}$ is properly shrunk; we assume that the last is accomplished. By ii) in Definition 4, $f(\cdot)$ can be extended from $\mathfrak{C}_\mathfrak{b}$ to a smooth function $f_\mathfrak{b}(\cdot)$

defined in an open neighborhood $O_{\mathfrak{b}}$ of $\overline{\mathfrak{C}_{\mathfrak{b}}}$. Finally, we define a map $q:\mathbb{R}^n\to\mathbb{R}^n$ by putting

$$q(h):=f'_{\mathfrak{b}}(x_*)h \qquad \text{whenever} \quad h\in K_{\mathfrak{b}} \text{ for some } \mathfrak{b}\in B, \tag{27}$$

where the r.h.s. uses the ordinary Jacobian matrix $f'_{\mathfrak{b}}(x_*)$.

Lemma 1: The map $q(\cdot)$ is well-defined.

Proof: Since $\bigcup_{\mathfrak{b}\in B}K_{\mathfrak{b}\in B}=\mathbb{R}^n$ thanks to i) in Definition 3, it suffices to show that

$$h\in K_{\mathfrak{b}^\dagger}\cap K_{\mathfrak{b}^\diamondsuit}\Rightarrow f'_{\mathfrak{b}^\dagger}(x_*)h=f'_{\mathfrak{b}^\diamondsuit}(x_*)h. \tag{28}$$

Let h meet the premises of this entailment. Then

$$I_h:=\{i\in I: h^\top\nabla g_i(x_*)=0\}\supset\{i\in I: b_i^\dagger\neq b_i^\diamondsuit\}. \tag{29}$$

By invoking i) in Definition 3 once more, we infer that $\mathcal{S}:=\{x\in\mathcal{O}: g_i(x)=0\ \forall i\in I_h\}$ is a smooth manifold in a vicinity of x_* and also that h is tangential to $\mathcal{S}$ at x_*. Hence there exists a parametric curve $\gamma(\theta),\theta\in[0,\delta],\delta>0$ such that

$$\mathcal{S}\ni\gamma(\theta)=x_*+\theta h+\circ(\theta).$$

So $g_i[\gamma(\cdot)]\equiv 0\ \forall i\in I_h$. If $i\in I\setminus I_h$, (26) and (29) yield that $b_i^\dagger=b_i^\diamondsuit$ and $b_i^\dagger h^\top\nabla g_i(x_*)<0$. It follows that $b_i^\dagger g_i[\gamma(\theta)]<0$ and $b_i^\diamondsuit g_i[\gamma(\theta)]<0$ for $\theta\approx 0$ and $i\in I\setminus I_h$. Overall, for $\theta\approx 0$, we have $b_i^\dagger g_i[\gamma(\theta)]\le 0$ and $b_i^\diamondsuit g_i[\gamma(\theta)]\le 0$ and so $\gamma(\theta)\in\overline{\mathfrak{C}_{\mathfrak{b}^\dagger}}\subset O_{\mathfrak{b}^\dagger}$, $\gamma(\theta)\in\overline{\mathfrak{C}_{\mathfrak{b}^\diamondsuit}}\subset O_{\mathfrak{b}^\diamondsuit}$. By the continuity argument

$$f(x)=f_{\mathfrak{b}}(x)\ \ \forall x\in\mathfrak{C}_{\mathfrak{b}}\Rightarrow f(x)=f_{\mathfrak{b}}(x)\ \ \forall x\in\overline{\mathfrak{C}_{\mathfrak{b}}}. \tag{30}$$

Thus, we see that

$$\begin{aligned} f[\gamma(\theta)]-f[x_*]&=f_{\mathfrak{b}^\dagger}[\gamma(\theta)]-f_{\mathfrak{b}^\dagger}[x_*]=\theta f'_{\mathfrak{b}^\dagger}(x_*)h+\circ(\theta),\\ f[\gamma(\theta)]-f[x_*]&=f_{\mathfrak{b}^\diamondsuit}[\gamma(\theta)]-f_{\mathfrak{b}^\diamondsuit}[x_*]=\theta f'_{\mathfrak{b}^\diamondsuit}(x_*)h+\circ(\theta).\end{aligned} \tag{31}$$

Therefore (28) is valid. □

Lemma 2: Any function $q(\cdot)$ satisfying Assumption 1 is globally Lipschitz continuous.

The proof is similar to Lemma 4.

Lemma 3: The map $q(\cdot)$ given by (27) is the differential of the map $f(\cdot)$ in the sense of Definition 5.

Proof: Suppose the contrary. By (26), (27), and Lemma 1, the map $q(\cdot)$ satisfies Assumption 1. So by Definition 6, (24) fails to be true: there exists $\delta>0$, an infinite sequence $\{h_j\}\subset S_0^1$ of unit vectors $\|h_j\|=1$ and a sequence $\{\theta_j\}\subset(0,\infty)$ such that

$$\begin{aligned} &A_j:=\frac{\left\|f(x_*+\theta_j h_j)-f(x_*)-\theta_j q(h_j)\right\|}{\theta_j}\ge\delta,\\ &\theta_j\to 0 \quad \text{as } j\to\infty.\end{aligned} \tag{32}$$

By passing to a proper subsequence, we can also ensure that there exist $h_\infty\in S_0^1$ and $\mathfrak{b}\in B$ such that

$$h_j\to h_\infty \quad \text{as } j\to\infty, \quad \text{and} \quad b_i g_i[x_*+\theta_j h_j]\le 0 \ \ \forall i\in I.$$

These and (26) imply that $h_\infty\in K_{\mathfrak{b}}$ and so $q(h_\infty)=f'_{\mathfrak{b}}(x_*)h_\infty$ by (27), whereas $x_*+\theta_j h_j\in\overline{\mathfrak{C}_{\mathfrak{b}}}\ \forall j$. Whence $f[x_*+\theta_j h_j]=f_{\mathfrak{b}}[x_*+\theta_j h_j]\ \forall j$ by (30). So

$$\begin{aligned} A_j&=\frac{\left\|f_{\mathfrak{b}}(x_*+\theta_j h_j)-f_{\mathfrak{b}}(x_*)-\theta_j q(h_\infty)+\theta_j[q(h_\infty)-q(h_j)]\right\|}{\theta_j}\\ &\le\frac{\left\|f_{\mathfrak{b}}(x_*+\theta_j h_j)-f_{\mathfrak{b}}(x_*)-\theta_j f'_{\mathfrak{b}}(x_*)h_\infty\right\|}{\theta_j}\\ &\quad+\left\|q(h_\infty)-q(h_j)\right\|\\ &\overset{\text{Lem. 2}}{\le}\frac{\left\|f_{\mathfrak{b}}(x_*+\theta_j h_j)-f_{\mathfrak{b}}(x_*)-\theta_j f'_{\mathfrak{b}}(x_*)h_\infty\right\|}{\theta_j}\\ &\quad+c\left\|h_\infty-h_j\right\|,\end{aligned}$$

which tends to zero as $j\to\infty$ in violation of (32). This contradiction completes the proof. □

Proof of Proposition 1: Is immediate from Lemma 3. □

C. Stability of the Steady State for the Piecewise-Smooth Function

Proposition 2: Suppose that Assumption 1 holds and the following claims are true:

i) *The origin 0 is the locally asymptotically stable equilibrium of the system (22);*
ii) *There exists a positively definite matrix $P=P^\top\in\mathbb{R}^{n\times n}$ and a conical q-related partition such that*

$$A_k^\top P A_k\le P \quad \forall k. \tag{33}$$

Then the origin is a globally asymptotically stable equilibrium of (22) and there exists a natural m and real $\eta\in(0,1)$ such that

$$V[q^m(x)]\le\eta V[x] \ \ \forall x\in\mathbb{R}^n, \quad \text{where} \quad V(x):=x^\top Px \tag{34}$$

and $q^m:=q\circ\cdots\circ q$ is the mth iteration of the map q.

The remainder of the section is devoted to the proof of Proposition 2, and so we posit that its assumptions are true. We also introduce the P-related Euclidean norm $\|x\|_P:=\sqrt{x^\top Px}$.

Lemma 4: The function $q(\cdot)$ is Lipschitz continuous and its Lipschitz constant with respect to $\|\cdot\|_P$ equals 1:

$$\|q(x_2)-q(x_1)\|_P\le\|x_2-x_1\|_P \ \ \forall x_i\in\mathbb{R}^n. \tag{35}$$

Proof: Whenever x_1,x_2 lie in a common domain P_k, (35) is straightforward from (33). By the continuity argument, this inequality extends on any $x_1,x_2\in\overline{P}_k$ from the closure $\overline{P}_k$ of P_k. For an arbitrary pair $x_1,x_2\in\mathbb{R}^n$, there exists a finite sequence $0=\theta_0<\theta_1<\ldots<\theta_s<\theta_{s+1}=1$ such that $x(\theta_i)$ and $x(\theta_{i+1})$ lie in a common domain $\overline{P}_{k(i)}$ for any $i=0,\ldots,s$, where $x(\theta):=(1-\theta)x_1+\theta x_2$. Since

$$\|q[x(\theta_{i+1})]-q[x(\theta_i)]\|_P\le\|x(\theta_{i+1})-x(\theta_i)\|_P, \quad \forall i=0,\ldots,s, \tag{36}$$

Then

$$\|q[x_2]-q[x_1]\|_P \le \sum_{i=0}^{s}\|x(\theta_{i+1})-x(\theta_i)\|_P \le \|x_2-x_1\|_P. \quad \square \tag{37}$$

It follows that for any natural m,

$$\|q^m(x_2)-q^m(x_1)\|_P \le \|x_2-x_1\|_P \quad \forall x_i \in \mathbb{R}^n. \tag{38}$$

Lemma 5: There exists a natural m and $\eta \in (0,1)$ such that (34) *holds.*

Proof: Since $x_t(\theta a)=\theta x_t(a)$ for all $t=0,1,\dots$ and $a\in\mathbb{R}^n$ by (23), assumption i) of Proposition 2 implies that

$$x_t(a)\to 0 \quad \text{as} \quad t\to\infty \quad \forall a\in\mathbb{R}^n. \tag{39}$$

Now we pick $\eta\in(0,1)$ and a finite $\sqrt{\eta}/2$-net $a_1,\dots,a_K\in S_0^1$ in the unit sphere $S_0^1:=\{x\in\mathbb{R}^n:\|x\|_P=1\}$: $x\in S_0^1 \Rightarrow \exists j=j(x)=1,\dots,K: \|x-a_j\|_P<\sqrt{\eta}/2$. Such a net does exist since the sphere is compact. Now we apply (39) to $a:=a_j$ and note that the convergence is uniform over the finite variety of j's. So there exists a natural m such that

$$\|q^t(a_j)\|_P=\|x_t(a_j)\|_P<\sqrt{\eta}/2 \quad \forall t\ge m,\ \ j=1,\dots,K.$$

Hence for $t\ge m$, we have

$$x\in S_0^1 \Rightarrow \|q^t(x)\|_P \le \|q^t(a_{j(x)})\|_P+\|q^t(a_{j(x)})-q^t(x)\|_P \overset{(38)}{<} \sqrt{\eta}/2+\|a_{j(x)}-x\|_P \le \sqrt{\eta}/2+\sqrt{\eta}/2=\sqrt{\eta}. \tag{40}$$

For $x=0$, (34) is clear. Let $x\ne 0$. Then $x/\|x\|_P\in S_0^1$ and so

$$\sqrt{\eta}\ge\left\|q^t\left(\frac{x}{\|x\|_P}\right)\right\|_P=\frac{\|q^t(x)\|}{\|x\|_P}\Rightarrow\|q^t(x)\|\le\sqrt{\eta}\|x\|_P,$$
$$V[q^t(x)]=\|q^t(x)\|^2\le\eta\|x\|_P^2=V(x).$$

Proof of Proposition 2: Whereas (34) holds by Lemma 5, the first claim of the proposition follows from (34). $\square$

Theorem 3: Suppose that the following claims hold:

- *A point $x_*\in O$ is an equilibrium for the discrete-time dynamical system*

$$x_{t+1}=f[x_t],\quad x_t\in\mathbb{R}^n,\quad t=0,1,\dots. \tag{41}$$

- *There exists a differential $q(\cdot)=f'(x_*)$ (in the sense of Definition 6) of $f(\cdot)$ at x_*;*
- *The properties* i) *and* ii) *from Proposition 2 hold for this differential.*

This theorem reduces analysis of stability of the primal nonlinear system to stability analysis of a simpler nonlinear system, which is piece-wise linear and positively homogeneous, unlike the primal one. We refer the reader to [42]–[47] for surveys of tools available for stability analysis of piecewise linear systems. Then the equilibrium x_* of the system (41) *is locally exponentially asymptotically stable.*

The proof of this theorem is prefaced by the following.

Lemma 6: For any natural m, the iteration $q^m(\cdot)$ is the differential of $f^m(\cdot)$.

Proof: We invoke the matrix P from ii) in Proposition 2 and the P-related norm $\|\cdot\|_P$. The proof will be via induction on m. For $m=1$, the claim is evident. Let it be true for some m, i.e., let

$$f^m(x)=\underbrace{f^m(x_*)}_{=x_*}+\Delta_x^m, \tag{42}$$

where

$$\Delta_x^m:=q^m(x-x_*)+\|x-x_*\|_P\alpha_m(x-x_*) \tag{43}$$

and

$$\alpha_m(h)\to 0 \quad \text{as} \quad h\to 0. \tag{44}$$

The rest of the proof follows from the fact that $q^m(\cdot)$ is continuous and positively homogeneous

$$\frac{\|f^{m+1}(x_*+h)-f(x_*)-q^{m+1}(h)\|_P}{\|h\|_P} \le \|\alpha_m(h)\|_P+\big[c_m+\|\alpha_m(h)\|_P\big]\|\alpha[\Delta^m_{x_*+h}]\|_P\to 0 \tag{45}$$

as $h\to 0$, which completes the proof. $\square$

Proof of Theorem 3: We invoke $P, V(\cdot), m$, and η from Proposition 2, and observe that

$$\begin{aligned} V[f^m(x)-x_*] &\overset{(44)}{=} V\big[q^m(x-x_*)+\|x-x_*\|_P\alpha_m(x-x_*)\big] \\ &\overset{(34)}{\le} V(x-x_*)\mathcal{K}, \\ \mathcal{K} &= \Big\{\eta+V\big[\alpha_m(x-x_*)\big]+2c_m\|\alpha_m(x-x_*)\|_P\Big\}. \end{aligned} \tag{46}$$

Now we pick $\overline{\eta}\in(\eta,1)$. By the continuity argument, there exists $\delta>0$ such that whenever $\|x-x_*\|_P<\delta$, we have $\mathcal{K}<\overline{\eta}$ and so $V[f^m(x)-x_*]\le\overline{\eta}V(x-x_*)$. Thus, we see that $x\mapsto V(x-x_*)$ is a strong Lyapunov function for the discrete-time dynamical system

$$x_{t+1}=f^m(x_t),\quad t=0,1,\dots. \tag{47}$$

By the second Lyapunov principle, there exist $\varkappa>0$ and $c>0$ such that

$$\|x_t^m(a)-x_*\|\le c\overline{\eta}^{t/2}\|a\| \quad \forall t\ge 0 \quad \text{whenever } \|a\|<\varkappa,$$

where $\{x_t^m(a)\}_t$ is the trajectory of (47) starting with $x_0^m=a$.

By Lemma 6, any iteration $f^k(\cdot)$ has a differential at the point x_*. Hence (44) imply existence of $\varepsilon_k>0$ and $c_k>0$ such that

$$\|f^k(x)-x_*\|\le c_k\|x-x_*\| \quad \text{whenever} \quad \|x-x_*\|<\varepsilon_k.$$

Now we put $c_0:=1$ and $\varepsilon:=\min\left\{\min_{k=1,\dots,m}\varepsilon_k;\min_{k=0,\dots,m}\frac{\varkappa}{c_k}\right\}$, $C:=c\max_{k=0,\dots,m}c_k$. Then whenever $\|a-x_*\|<\varepsilon$, we have $\|f^k(a)-x_*\|<\varkappa\ \forall k=0,\dots,m$ and so

$$\begin{aligned} \|x_\tau^m[f^k(a)]-x_*\| &\le c\overline{\eta}^{\tau/2}\|f^k(a)-x_*\| \\ &\le cc_k\overline{\eta}^{\tau/2}\|a-x_*\|=C\overline{\eta}^{\tau/2}\|a-x_*\| \\ &\forall\tau\ge 0,\quad k=0,\dots,m. \end{aligned} \tag{48}$$

Let $x_t(a)$ stand for the trajectory of (41) that starts with $x_0(a)=a$ and $\lfloor\cdot\rfloor$ for the integer floor. Then $x_t(a)=$

$x^m_{\lfloor t/m \rfloor}[f^{t-m\lfloor t/m \rfloor}(a)]$ and so

$$\|x_t(a) - x_*\| = \left\| x^m_{\lfloor t/m \rfloor}[f^{t-m\lfloor t/m \rfloor}(a)] - x_* \right\| \leq \frac{C}{\sqrt{\overline{\eta}}}(\sqrt{\overline{\eta}})^{t/m}\|a - x_*\| \leq C_*\eta_*^t\|a - x_*\|, \tag{49}$$

where $C_* := \frac{C}{\sqrt{\overline{\eta}}}$ and $\eta_* := (\overline{\eta})^{1/(2m)} \in (0, 1)$. This completes the proof. □

APPENDIX B
PROOF OF THEOREM 1

Stability analysis of the zero steady state of model (14) is studied by applying theorem 3 from in Appendix A. In subsection B-A we show that the right-hand side of (14) is piecewise smooth. In subsection B-B system (14) is linearized (resulting in piecewise-linear map). In subsection B-C stability of the origin for linearized system is studied. In subsection B-D stability of the linearized system is used to prove stability of the origin for non-linear system.

A. Piecewise-Smoothness of the Right-Hand Side

It is easy to see, that the right-hand side of (14) $f : \mathcal{O} \subset \mathbb{R}^2 \to \mathbb{R}^2$ satisfies the conditions 1)–3) for piecewise smooth function in a small neighborhood $\mathcal{O}$ of the origin (see Definition 4, Appendix A):

1) The function $f(\cdot)$ is continuous in a small neighborhood $\mathcal{O}$ of equilirbium $(0, 0)$;
2) From (14) in a small neighborhood of equilibrium $\mathcal{O}$ there are three curves S_1, S_2, S_3 dividing the phase space:
   - S_1: $p_k = 0$;
   - S_2: $p_k > 0$, $c_k = 0$; $u_k = \frac{p_k}{1-p_k}$ for $0 < p_k < 1$;
   - S_3: $p_k < 0$, $l_k = 1$.

   The function $f(\cdot)$ is continuously differentiable on any connected component $\mathfrak{C}$ of the set $\mathcal{O} \setminus \left[S_1 \cup S_2 \cup S_3\right]$ and, moreover, can be extended from $\mathfrak{C}$ to an open neighborhood of the closure $\overline{\mathfrak{C}}$ with retaining this smoothness;
3) The curves S_1, S_2, and S_3 are mutually non-tangential on $\mathcal{O}$.

B. Linearization

One can compute the differential $q(\cdot)$ of $f(\cdot)$ (see Definition 6 and Proposition 1, Appendix A) as follows:

$$x_{k+1} = q(x_k) = A_j x_k, \quad x_k \in R_j, \quad j = 1, 2, 3, 4,$$
$$A_1 = \frac{1}{1+\alpha}\begin{bmatrix} 1 & -1 \\ 2\beta & 1+\alpha-2\beta \end{bmatrix},$$
$$A_2 = \begin{bmatrix} 1-\alpha & -1 \\ 2\beta(1-\alpha) & 1-2\beta \end{bmatrix},$$
$$A_3 = \begin{bmatrix} 1 & -1 \\ 2\beta & 1-2\beta \end{bmatrix},$$
$$A_4 = \frac{1}{\alpha+1}\begin{bmatrix} 1-\alpha & -1 \\ 2\beta(1-\alpha) & 1+\alpha-2\beta \end{bmatrix}, \tag{50}$$

where the lines L_1, L_2, L_3 separating conical regions P_j are defined by equations conical partitioning:

- L_1: $p_k = 0$;
- L_2: $p_k \geq 0$, $u_k = p_k$;
- L_3: $p_k \leq 0$, $u_k = (1-\alpha)p_k$.

C. Stability of the Linearized System

Consider linearized system (50) and the quadratic Lyapunov function

$$V(x) = x^T H x, \quad H = \begin{bmatrix} 2\beta & -\beta \\ -\beta & 1 \end{bmatrix}. \tag{51}$$

One can check that $V(x)$ is positive definite for $0 < \beta < 2$ and is non-increasing along the trajectories of the linearized system:

- $x \in P_1$: $V(q(x)) - V(x) = -x^T \frac{2\beta\alpha}{(1+\alpha)^2}\begin{pmatrix} 1 & -1 \\ -1 & 1 \end{pmatrix} x \leq 0$,
- $x \in P_2$: $V(q(x)) - V(x) = -x^T \begin{pmatrix} 2\beta\alpha & 0 \\ 0 & 0 \end{pmatrix} x \leq 0$,
- $x \in P_3$: $V(q(x)) - V(x) = 0$,
- $x \in P_4$: $V(q(x)) - V(x) = -x^T \frac{2\alpha\beta}{(1+a)^2}\begin{pmatrix} 4 & -2 \\ -2 & 1 \end{pmatrix} x \leq 0$.

Thus, the origin of the linearized system is stable. The exponential stability of the origin for $0 < \beta < 2$, $\beta \neq \frac{3}{2}$ can be proved using discrete-time analog of the LaSalle invariance principle (see, e.g. [48]). First, we define a set

$$E = \{x | V(x) = V(q(x))\}, \tag{52}$$

and show that $V(x) = V(q(x))$ for $x_k \in E = P_3 \cup y_1$, where y_1 is a ray

$$y_1 = \{x | x \in r[-1, -2]^T, \quad r \geq 0\}. \tag{53}$$

Then we seek for the largest positively invariant set $M \subset E$. For $0 < \beta < 2$, $\beta \neq \frac{3}{2}$ one obtains $M = \{0\}$ and for $\beta = \frac{3}{2}$ the set M is comprised of three rays (the lower and upper boundaries of S_3 and a special ray y_1). Thus, the origin is asymptotically stable for $0 < \beta < 2$, $\beta \neq \frac{3}{2}$.

D. Local Stability of the Nonlinear System

Now we have the following:

- The origin is an equilibrium for the discrete-time dynamical system $x_{k+1} = f(x_k)$;
- There exists the differential $q(\cdot) = f'(x_*)$ (in the sense of Definition 6) of the function $f(\cdot)$ at $(0, 0)$;
- The linearized system is asymptotically stable (see properties i) and ii) from Proposition 2, Appendix A).

Then, Theorem 3 from Appendix A yields that the origin of system (14) is uniformly exponentially stable for $0 < \beta < 2$, $\beta \neq \frac{3}{2}$, $0 < \alpha < 1$. Note that for $\beta = \frac{3}{2}$ there is infinite number of period-3 limit cycles in linearized system (50), while these limit cycles are non-existent in nonlinear system (14). Simulation shows, that the origin of the nonlinear system is locally stable for $\beta = \frac{3}{2}$.

APPENDIX C
INSTABILITY FOR $\alpha > 0$, $\beta > 2$

Here we use Lemma 5 from [17] to show that there is a trajectory of linearized system (50) diverging from the origin.

It is easy to see, that the eigenvalues of A_4A_3 are real, distinct, and larger eigenvalue $\lambda_1 > 1$ has an associated eigenvector x_1 in the right-hand canonical form with the slope $\mu = (\lambda_1(a+1) + (a+2\beta-1))/(a_2\beta - 2)$. Since $\mu > 1$ we get $x_1 \in P_3$. Therefore,

$$A_3 x_1 = (\mu - 1) \begin{bmatrix} -1 \\ \frac{2\beta + \mu(1-2\beta)}{\mu - 1} \end{bmatrix}. \tag{54}$$

Since $(2\beta + \mu(1-2\beta))/(\mu - 1) < \alpha - 1$, that is $\mu > (\lambda_1(a+1) + (a+2\beta-1))/(a_2\beta - 2)$, we get $A_3x_1 \in P_4$. Accordingly, trajectory starting at $x_1 \in P_3$ goes in one step to $A_3x_1 \in P_4$ and in one further step to $A_4A_3x_1 = \lambda_1\, x_1 \in P_3$, because λ_1 is real and positive. As $\lambda_1 > 1$, it is clear that the resulting orbit diverges.

ACKNOWLEDGMENT

The authors would like to thank Giovanni Bianchi (Advantest Corporation) for valuable comments and discussions on practical realizations of CP-PLL.

REFERENCES

[1] E. Kaplan and C. Hegarty, *Understanding GPS: Principles and Applications*. Norwood, MA, USA: Artech House, 2006.

[2] J. Proakis and M. Salehi, *Digital Communications*. New York, NY, USA: McGraw-Hill, 2008.

[3] K. Du and M. Swamy, *Wireless Communication Systems: From RF Subsystems to 4G Enabling Technologies*. Cambridge, U.K.: Cambridge Univ. Press, 2010.

[4] G. Bianchi, *Phase-Locked Loop Synthesizer Simulation*. New York, NY, USA: McGraw-Hill, 2005.

[5] F. M. Gardner, "Charge-pump phase-lock loops," *IEEE Trans. Commun.*, vol. COM-28, no. 11, pp. 1849–1858, Nov. 1980.

[6] J. P. Hein and J. W. Scott, "Z-domain model for discrete-time PLL's," *IEEE Trans. Circuits Syst.*, vol. 35, no. 11, pp. 1393–1400, Nov. 1988.

[7] J. Lu, B. Grung, S. Anderson, and S. Rokhsaz, "Discrete Z-domain analysis of high order phase locked loops," in *Proc. IEEE Int. Symp. Circuits Syst.*, vol. 1, May 2001, pp. 260–263.

[8] M. Van Paemel, "Analysis of a charge-pump PLL: A new model," *IEEE Trans. Commun.*, vol. 42, no. 7, pp. 2490–2498, Jul. 1994.

[9] D. Gillespie, M. Kennedy, and G. Kolumban, "Improved nonlinear model of a second-order charge-pump PLL," in *Nonlinear Dynamics of Electronic Systems*. Singapore: World Scientific, 2000, pp. 240–243.

[10] N. Kuznetsov *et al.*, "Charge pump phase-locked loop with phase-frequency detector: Closed form mathematical model," 2019, *arXiv:1901.01468*. [Online]. Available: https://arxiv.org/abs/1901.01468

[11] N. V. Kuznetsov, M. Y. Lobachev, M. V. Yuldashev, and R. V. Yuldashev, "The Egan problem on the pull-in range of type 2 PLLs," *IEEE Trans. Circuits Syst. II, Exp. Briefs*, vol. 68, no. 4, pp. 1467–1471, Apr. 2021.

[12] N. V. Kuznetsov, G. A. Leonov, M. V. Yuldashev, and R. V. Yuldashev, "Rigorous mathematical definitions of the hold-in and pull-in ranges for phase-locked loops," *IFAC-PapersOnLine*, vol. 48, no. 11, pp. 710–713, 2015.

[13] G. A. Leonov, N. V. Kuznetsov, M. V. Yuldashev, and R. V. Yuldashev, "Hold-in, pull-in, and lock-in ranges of PLL circuits: Rigorous mathematical definitions and limitations of classical theory," *IEEE Trans. Circuits Syst. I, Reg. Papers*, vol. 62, no. 10, pp. 2454–2464, Oct. 2015.

[14] R. E. Best, N. V. Kuznetsov, G. A. Leonov, M. V. Yuldashev, and R. V. Yuldashev, "Tutorial on dynamic analysis of the Costas loop," *Annu. Rev. Control*, vol. 42, pp. 27–49, 2016.

[15] N. V. Kuznetsov, M. Y. Lobachev, M. V. Yuldashev, and R. V. Yuldashev, "On the Gardner problem for phase-locked loops," *Doklady Math.*, vol. 100, no. 3, pp. 568–570, Nov. 2019.

[16] N. V. Kuznetsov, A. S. Matveev, M. V. Yuldashev, R. V. Yuldashev, and G. Bianchi, "Stability of charge-pump phase-locked loops: The hold-in and pull-in ranges," *IFAC-PapersOnLine*, vol. 53, no. 2, pp. 2022–2026, 2020.

[17] P. F. Curran, C. Bi, and O. Feely, "Dynamics of charge-pump phase-locked loops," *Int. J. Circuit Theory Appl.*, vol. 41, no. 11, pp. 1109–1135, Nov. 2013.

[18] C. Hedayat, A. Hachem, Y. Leduc, and G. Benbassat, "Modeling and characterization of the 3rd order charge-pump PLL: A fully event-driven approach," *Anal. Integr. Circuits Signal Process.*, vol. 19, no. 1, pp. 25–45, 1999.

[19] T. Johnson and J. Holmberg, "Nonlinear state-space model of charge-pump based frequency synthesizers," in *Proc. IEEE Int. Symp. Circuits Syst. (ISCAS)*, May 2005, pp. 4469–4472.

[20] Z. Wang, "An analysis of charge-pump phase-locked loops," *IEEE Trans. Circuits Syst. I, Reg. Papers*, vol. 52, no. 10, pp. 2128–2138, Oct. 2005.

[21] B. Daniels, "Analysis and design of high order digital phase locked loops," Ph.D. dissertation, Dept. Electron. Eng., Nat. Univ. Ireland Maynooth, Maynooth, Ireland, 2008.

[22] M. Guermandi, E. Franchi, and A. Gnudi, "On the simulation of fast settling charge pump PLLs up to fourth order," *Int. J. Circuit Theory Appl.*, vol. 39, no. 12, pp. 1257–1273, Dec. 2011.

[23] F. Bizzarri, A. Brambilla, and G. S. Gajani, "Periodic small signal analysis of a wide class of type-II phase locked loops through an exhaustive variational model," *IEEE Trans. Circuits Syst. I, Reg. Papers*, vol. 59, no. 10, pp. 2221–2231, Oct. 2012.

[24] B. I. Shakhtarin, A. A. Timofeev, and V. V. Sizykh, "Mathematical model of the phase-locked loop with a current detector," *J. Commun. Technol. Electron.*, vol. 59, no. 10, pp. 1061–1068, Oct. 2014.

[25] C. Hangmann, C. Hedayat, and U. Hilleringmann, "Stability analysis of a charge pump phase-locked loop using autonomous difference equations," *IEEE Trans. Circuits Syst. I, Reg. Papers*, vol. 61, no. 9, pp. 2569–2577, Sep. 2014.

[26] N. Kuznetsov *et al.*, "Comments on van Paemel's mathematical model of charge-pump phase-locked loop," *Differ. Uravnenia i Protsesy Upravlenia*, no. 1, pp. 109–120, 2019. [Online]. Available: https://diffjournal.spbu.ru/pdf/19107-jdecp-kuznetsov.pdf

[27] F. Gardner, *Phaselock Techniques*, 3rd ed. New York, NY, USA: Wiley, 2005.

[28] P. Acco, "Study of the loop 'a phase lock: Hybrid aspects taken into account," Ph.D. dissertation, INSA, Toulouse, France, 2003.

[29] O. Feely, "Nonlinear dynamics of discrete-time circuits: A survey," *Int. J. Circuit Theory Appl.*, vol. 35, nos. 5–6, pp. 515–531, 2007.

[30] W. Egan, *Frequency Synthesis by Phase Lock*, 1st ed. New York, NY, USA: Wiley, 1981.

[31] N. V. Kuznetsov, M. Y. Lobachev, M. V. Yuldashev, R. V. Yuldashev, and G. Kolumbán, "Harmonic balance analysis of pull-in range and oscillatory behavior of third-order type 2 analog PLLs," *IFAC-PapersOnLine*, vol. 53, no. 2, pp. 6378–6383, 2020.

[32] A. Fahim, *Clock Generators for SOC Processors: Circuits and Architectures*. Boston, MA, USA: Kluwer, 2005.

[33] K. Shu and E. Sánchez-Sinencio, *CMOS PLL Synthesizers: Analysis and Design*, vol. 783. Berlin, Germany: Springer, 2006.

[34] B. Razavi, *Monolithic Phase-Locked Loops and Clock Recovery Circuits: Theory and Design*. Hoboken, NJ, USA: Wiley, 1996.

[35] K. D. Alexandrov, N. V. Kuznetsov, G. A. Leonov, P. Neittaanmäki, and S. M. Seledzhi, "Pull-in range of the classical PLL with impulse signals," *IFAC-PapersOnLine*, vol. 48, no. 1, pp. 562–567, 2015.

[36] A. Homayoun and B. Razavi, "On the stability of charge-pump phase-locked loops," *IEEE Trans. Circuits Syst. I, Reg. Papers*, vol. 63, no. 6, pp. 741–750, Jun. 2016.

[37] G. Leonov and N. Kuznetsov, "Hidden attractors in dynamical systems. From hidden oscillations in Hilbert–Kolmogorov, Aizerman, and Kalman problems to hidden chaotic attractors in Chua circuits," *Int. J. Bifurcation Chaos Appl. Sci. Eng.*, vol. 23, no. 1, Jan. 2013, Art. no. 1330002.

[38] N. V. Kuznetsov, "Theory of hidden oscillations and stability of control systems," *J. Comput. Syst. Sci. Int.*, vol. 59, no. 5, pp. 647–668, Sep. 2020.

[39] G. Bianchi, N. V. Kuznetsov, G. A. Leonov, S. M. Seledzhi, M. V. Yuldashev, and R. V. Yuldashev, "Hidden oscillations in SPICE simulation of two-phase Costas loop with non-linear VCO," *IFAC-PapersOnLine*, vol. 49, no. 14, pp. 45–50, 2016.

[40] N. V. Kuznetsov, G. A. Leonov, M. V. Yuldashev, and R. V. Yuldashev, "Hidden attractors in dynamical models of phase-locked loop circuits: Limitations of simulation in MATLAB and SPICE," *Commun. Nonlinear Sci. Numer. Simul.*, vol. 51, pp. 39–49, Oct. 2017.
[41] N. V. Kuznetsov *et al.*, "The birth of the global stability theory and the theory of hidden oscillations," in *Proc. Eur. Control Conf. (ECC)*, May 2020, pp. 769–774.
[42] G. Feng, "Stability analysis of piecewise discrete-time linear systems," *IEEE Trans. Autom. Control*, vol. 47, no. 7, pp. 1108–1112, Jul. 2002.
[43] L. B. Groff, G. Valmórbida, and J. M. G. da Silva, "Stability analysis of piecewise affine discrete-time systems," in *Proc. IEEE 58th Conf. Decis. Control (CDC)*, Dec. 2019, pp. 8172–8177.
[44] R. Iervolino, F. Vasca, and L. Iannelli, "Cone-copositive piecewise quadratic Lyapunov functions for conewise linear systems," *IEEE Trans. Autom. Control*, vol. 60, no. 11, pp. 3077–3082, Nov. 2015.
[45] K. Liu, J. Hu, Y. Yao, B. Yang, and X. Huo, "Stability analysis of discrete-time piecewise-linear systems: A generating function approach," *Int. J. Control, Autom. Syst.*, vol. 12, no. 5, pp. 1005–1010, Oct. 2014.
[46] Z. Sun, "Stability of piecewise linear systems revisited," *Annu. Rev. Control*, vol. 34, no. 2, pp. 221–231, Dec. 2010.
[47] S. Waitman. (Jul. 2018). *A Piecewise-Affine Approach to Nonlinear Performance*. Theses, Université de Lyon. [Online]. Available: https://tel.archives-ouvertes.fr/tel-01917511
[48] N. Bof, R. Carli, and L. Schenato, "Lyapunov theory for discrete time systems," 2018, *arXiv:1809.05289*. [Online]. Available: https://arxiv.org/abs/1809.05289

Nikolay Kuznetsov graduated from Saint-Petersburg State University, Russia, in 2001. He received the Candidate of Science and the Doctor of Science degrees from Saint-Petersburg State University in 2004 and 2016, respectively, and the Ph.D. degree from the University of Jyväskylä, Finland, in 2008. From 2018, the research group chaired by Prof. Kuznetsov has awarded the status of the Leading Scientific School (Center of Excellence) of Russia in the field of mathematics and mechanics. He was named as a Professor of the Year in the field of mathematics in Russia in 2020. He is currently a Professor and the Head of the Department of Applied Cybernetics, Saint-Petersburg State University. He is also a Visiting Professor and the Co-Chair of the Finnish-Russian Educational & Research Program organized together with Saint-Petersburg State University. He was elected as a Foreign Member of the Finnish Academy of Science and Letters in 2020. Since 2018, he has been the Head of the Laboratory of Information and Control Systems, Institute for Problems in Mechanical Engineering, Russian Academy of Science. His research interests include nonlinear control systems, stability and oscillations in dynamical systems, theory of hidden oscillations, hidden attractors, and phase-locked loop nonlinear analysis.

Alexey Matveev was born in Leningrad, Russia, in 1954. He received the M.S. degree in applied mathematics and the Ph.D. degree in engineering cybernetics from Leningrad University, St. Petersburg, Russia, in 1976 and 1980, respectively.

He is currently a Professor with the Department of Mathematics and Mechanics, Saint-Petersburg State University. His research interests include control over communication networks, hybrid dynamical systems, and navigation and control of mobile robots.

Marat Yuldashev received the Candidate degree from Saint-Petersburg State University, Russia, in 2013, and the Ph.D. degree from the University of Jyväskylä, Finland, in 2013, in the framework of joint Russian-Finnish Ph.D. Program. He is currently a Professor with Saint-Petersburg State University. His research interests include nonlinear models of phase-locked loops and Costas loops, and SPICE simulation.

Renat Yuldashev received the Candidate degree from Saint-Petersburg State University, Russia, in 2013, and the Ph.D. degree from the University of Jyväskylä, Finland, in 2013, in the framework of joint Russian-Finnish Ph.D. Program. He is currently a Professor with Saint-Petersburg State University. His research interests include synchronization of power converters in electrical grids and nonlinear analysis of PLLs.